Monthly Notices of the ROYAL ASTRONOMICAL SOCIETY

MNRAS **534,** L1–L6 (2024) https://doi.org/10.1093/mnrasl/slae071
Advance Access publication 2024 July 27

A tight N/O–potential relation in star-forming galaxies

N. Boardman [1]★ V. Wild[1] and N. Vale Asari [2]

[1]*School of Physics and Astronomy, University of St Andrews, North Haugh, St Andrews KY16 9SS, UK*
[2]*Departamento de Física–CFM, Universidade Federal de Santa Catarina, C.P. 5064, 88035-972 Florianópolis, SC, Brazil*

Accepted 2024 July 21. Received 2024 July 19; in original form 2024 June 21

ABSTRACT

We report a significantly tighter trend between gaseous N/O and M_*/R_e (a proxy for gravitational potential) than has previously been reported between gaseous metallicity and M_*/R_e, for star-forming galaxies in the Mapping Nearby Galaxies at Apache Point Observatory (MaNGA) survey. We argue this result to be a consequence of deeper potential wells conferring greater resistance to metal outflows while also being associated with earlier star-formation histories, combined with N/O being comparatively unaffected by metal-poor inflows. The potential–N/O relation thus appears to be both more resistant to short time-scale baryonic processes and also more reflective of a galaxy's chemical evolution state, when compared to previously considered relations.

Key words: ISM: abundances – ISM: general – ISM: evolution – galaxies: ISM – galaxies: statistics – galaxies: abundances.

1 INTRODUCTION

The question of chemical evolution remains at the heart of observational galaxy astrophysics. The chemistry of galaxies' stars and gas have been studied in much detail, in terms of both metallicities and in terms of elemental abundance ratios. For stars, the most frequently considered abundance measures are [Fe/H] and [α/Fe]; for gas, the most common measures are instead 12 + log(O/H) and log(N/O). In both cases, combining measures yields much more information than does any one measure alone, due to the different enrichment time-scales involved. Alpha elements such as oxygen are released into the ISM via Type-II supernovae, resulting in enrichment on just ∼10 Myr time-scales after a star-formation event (e.g. Timmes, Woosley & Weaver 1995); iron and nitrogen meanwhile are released on much longer time-scales, largely by Type-Ia supernovae and by AGB stars, respectively (see Maiolino & Mannucci 2019, for a review). N/O and metallicity have been shown repeatedly to be tightly correlated at higher metallicities, with N/O instead displaying a near-constant value in low-metallicity objects (e.g. Pilyugin, Vílchez & Thuan 2010; Andrews & Martini 2013; Pérez-Montero et al. 2016).

Scaling relations provide important constraints for chemical evolution models and thus provide important insight into the relevant physics. Of particular importance is the mass–metallicity relation, in which metallicity rises with increasing stellar mass (M_*), which has been noted repeatedly for both stellar and gaseous metallicities (e.g. Lequeux et al. 1979; Tremonti et al. 2004; Gallazzi et al. 2005; Kewley & Ellison 2008). The gaseous mass–metallicity relation flattens at high masses, potentially indicating such galaxies to have reached a metallicity equilibrium (e.g. Lilly et al. 2013; Belfiore et al. 2019b). More compact galaxies have also been reported to be more metal-rich at a given stellar mass in both observations (e.g. Ellison et al. 2008; McDermid et al. 2015; Li et al. 2018) and simulations (Ma et al. 2024), with galaxies' size typically parametrized using the half-light radius R_e, and more compact galaxies also appear to possess flatter metallicity gradients over a wide range of stellar masses (Boardman et al. 2021, 2022). The parameter M_*/R_e (hereafter Φ_e) has been reported to correlate particularly tightly with galaxies' stellar or gaseous metallicities, with M_* and M_*/R_e^2 (hereafter Σ_e) producing looser correlations by comparison (Barone et al. 2018, 2020, 2022; D'Eugenio et al. 2018; Vaughan et al. 2022; Ma et al. 2024; Sánchez-Menguiano et al. 2024). This has been repeatedly interpreted as reflecting the importance of gravitational potential, for which Φ_e is considered a proxy; in this scenario, higher gravitational potentials confer greater resistance to metal-loss via outflows, resulting in great chemical enrichment in more compact systems. Baker & Maiolino (2023) have however challenged this interpretation, reporting a comparatively weak metallicity trend when dynamical mass is considered instead of stellar mass.

In this letter, we report a particularly tight correlation between log(N/O) and Φ_e, using data from the SDSS-IV Mapping Nearby Galaxies at Apache Point Observatory (MaNGA) integral-field unit (IFU) survey. We further report that Φ_e correlates more tightly with log(N/O) than with gaseous metallicity, with the Φ_e–metallicity correlation largely disappearing once log(N/O) is accounted for. We present our sample and data in Section 2, and our results in Section 3. We discuss our findings and conclude in Section 4. We use 'metallicity' to refer to gas-phase metallicities 12 + log(O/H), assume a Chabrier (2003) initial mass function and adopt the following Λ cold dark matter cosmology: $H_0 = 71$ km/s/Mpc, $\Omega_M = 0.27$, $\Omega_\Lambda = 0.73$.

2 SAMPLE & DATA

We draw our parent galaxy sample from the SDSS-IV MaNGA survey (Bundy et al. 2015), for which all data is publicly available as of SDSS Data Release 17 (DR17; Abdurro'uf et al. 2022). The MaNGA survey performed IFU spectroscopic observations on ∼10000 galaxies out to redshifts $z \lesssim 0.15$ (Yan et al. 2016b; Wake et al. 2017), with the main MaNGA sample selected to possess a

★ E-mail: nfb@st-andrews.ac.uk

roughly flat distribution in $\log(M_*)$. The observations were carried out with the two Baryon Oscillation Spectroscopic Survey (BOSS) spectrographs at Apache Point Observatory (Gunn et al. 2006; Smee et al. 2013). The MaNGA IFUs consist of hexagonal optical fibre bundles containing 19–127 fibres of 2″ diameter apiece (Law et al. 2016), with three-point dithers employed to fully sample the field of view (Drory et al. 2015; Law et al. 2015). The observations were reduced with the MaNGA Data Reduction Pipeline (Yan et al. 2016a; Law et al. 2016, 2021), prior to analysis with the MaNGA Data Analysis Pipeline (DAP; Belfiore et al. 2019a; Westfall et al. 2019; Law et al. 2021). MaNGA data and analysis products are available on the SDSS science archive server[1] and can also be accessed using the Marvin interface (Cherinka et al. 2019).

We obtained values of axis ratio (b/a), R_e, and M_* from the NASA-Sloan-Atlas (NSA) catalogue (Blanton et al. 2011),[2] where R_e and b/a are elliptical Petrosian values. We restrict to MaNGA galaxies in the Primary + and Secondary samples, which were observed out to $\sim$1.5 R_e and $\sim$2.5 R_e respectively, and we further restrict to galaxies with observed axis ratios $b/a > 0.6$. We adopt 0.1 dex uncertainties on M_*, representative of typical M_* uncertainties in the MPA-JHU catalogue,[3] while assuming 0.05 dex uncertainties on R_e (D'Eugenio et al. 2018); this results in M_* dominating the uncertainties on Φ_e and Σ_e.

We obtained emission line maps from the DAP, extracting fluxes and errors for the following features: H α, H β, [O III]$_{5008}$, [N II]$_{6585}$, [S II]$_{6718}$, [S II]$_{6733}$ and [O II]$_{3737,3729}$. These are corrected by the DAP for Milky Way foreground extinction (Belfiore et al. 2019a, Section 2.2.3), by applying the O'Donnell (1994) reddening law to the maps of Schlegel, Finkbeiner & Davis (1998). We also extracted H α equivalent widths ($EW_{H\alpha}$) from the DAP. We used DAP emission line values from non-parametric summed fluxes in all cases. We restricted to spaxels for which $S/N > 3$ for all obtained emission line fluxes. We corrected emission lines for dust using a Fitzpatrick et al. (2019) correction curve, assuming an intrinsic Balmer decrement H α/H $\beta = 2.86$.

We selected star-forming spaxels by employing BPT diagnostics (Baldwin, Phillips & Terlevich 1981; Osterbrock & Pogge 1985; Veilleux & Osterbrock 1987) and by requiring that $EW_{H\alpha} > 14$ Å, with the latter requirement serving to avoid galaxies with significant diffuse ionized gas (DIG) contamination in their studied regions (Lacerda et al. 2018; Vale Asari et al. 2019). For BPT criteria, we used the Kauffmann et al. (2003) BPT-N II demarcation line and the Kewley et al. (2001) BPT-S II demarcation line.

We estimated gas metallicities for all star-forming spaxels using the RS32 calibrator of Curti et al. (2020). The RS32 indicator is defined as [S II]$_{6718,6733}$/H α + [O III]$_{5008}$/H β, wherein all ratios have been corrected for dust. We estimate spaxels' log(N/O) using the Florido, Zurita & Pérez-Montero (2022) N2O2 calibrator (their equation 1), wherein N2O2 is defined as [N II]$_{6585}$/[O II]$_{3737,3729}$ (likewise corrected for dust). The RS32 indicator is double-valued; we therefore assumed all spaxels to be on the upper metallicity branch, while discarding spaxels with RS32 values beyond the Curti et al. (2020) fitted range.

We then selected a sample of galaxies for which characteristic chemical abundances can be obtained. Specifically, we aimed to estimate the gas metallicity at 1 R_e, $12 + \log(O/H)_e$, along with the 1 R_e N/O abundance $\log(N/O)_e$. Values at 1 R_e have been shown to be representative of galaxies' global properties relating to both stars and gas (González Delgado et al. 2014, 2015; Sánchez et al. 2016b), making them useful as characteristic values. We select our sample by first requiring galaxies to possess at least 40 star-forming spaxels over galactocentric radii 0.5–1.5 R_e with at least 20 spaxels on either side of the midpoint; this produces a sample of 2070 galaxies. We then grouped a given galaxy's spaxels into a series of elliptical annuli of width 0.1 R_e, covering 0.5–1.5 R_e. We required a minimum of 5 star-forming spaxels per annulus, while also requiring at least 3 annuli in total with coverage on both sides of 1 R_e; we found all 2070 sample galaxies to meet these criteria.

We computed galaxies' radial profiles in log(N/O) and $12 + \log(O/H)$ over 0.5–1.5 R_e by calculating the median log(N/O) and $12 + \log(O/H)$ within each annulus for a given galaxy, before performing an unweighted straight line fit with the IDL LINFIT routine. We used these fits to obtain galaxies' abundances at 1 R_e. Our overall methodology is similar to that employed in the MaNGA pipe3d value-added catalogue for gas-phase abundances (Sánchez et al. 2016a, b, 2018, 2022), though we note that our higher $EW_{H\alpha}$ cut provides somewhat greater resistance to DIG contamination.

We obtained errors on our abundances by performing 100 Monte Carlo simulations of each straight-line fit with bootstrapped residuals, with errors reported as the standard deviations from the Monte Carlo fits. Our obtained errors on $12 + \log(O/H)_e$ and $\log(N/O)_e$ are small: we find median errors of just 0.002 dex and 0.005 dex, respectively, indicating the measured abundances to be highly precise. This occurs due to the large number of star-forming spaxels – typically hundreds – that most of our sample galaxies possess, with all ten annuli included in most cases. Considerable systematic uncertainty arises from variations between calibrators (e.g. Kewley & Ellison 2008; Scudder et al. 2021; Florido et al. 2022), meaning that *absolute* values of abundances will be much more uncertain than *relative* values of abundances across our sample.

For comparison, we also obtained abundances at 1 R_e by computing radial profiles directly from galaxies' spaxel maps without employing annuli, which were again fit with LINFIT. We found these to produce entirely equivalent results to those from the annulus-based abundances. Thus, we focus on the annulus-based values for the remainder of this article.

We present the parent and final samples in terms of mass and star formation rate (SFR) in Figure 1, which demonstrates our sample selection to implicitly favour galaxies with significant ongoing star-formation. We obtained SFRs from the *log_sfr_ssp* column in the Pipe3d summary catalogue (Sánchez et al. 2022), in which SFRs are derived from spectral fits over the full MaNGA field of view, and we adjusted these SFRs to a Chabrier IMF.

3 RESULTS

In Figure 2, we plot $\log(N/O)_e$ and $12 + \log(O/H)_e$, as functions of M_*, Φ_e, and Σ_e. We also give the corresponding Spearman correlation coefficients ρ, with p-value $P \ll 0.01$ for all quoted values. We find both N/O and metallicity to correlate most tightly with Φ_e, as has been noted for metallicity previously (D'Eugenio et al. 2018; Sánchez-Menguiano et al. 2024). We further find that N/O correlates more tightly with all three parameters (M_*, Φ_e, and Σ_e) than does metallicity. Similarly to D'Eugenio et al. (2018), we colour our data points by R_e; we see clear residual size dependencies when plotting abundances against M_* or Σ_e, further emphasising that Φ_e is the more predictive parameter.

In Figure 3, we consider Φ_e in chemical space by presenting it as a combined function of $12 + \log(O/H)_e$ and $\log(N/O)_e$; the lower

[1] https://data.sdss.org/sas/
[2] https://data.sdss.org/sas/dr17/sdss/atlas/v1/nsa_v1_0_1.fits
[3] Obtained from https://www.sdss4.org/dr17/spectro/galaxy_mpajhu/

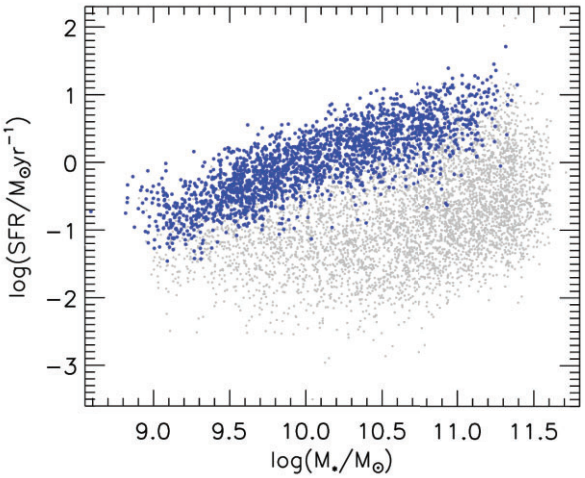

Figure 1. Selected sample (large blue points) and MaNGA parent sample (small grey points) in terms of stellar mass ($h = 0.71$) and SFR (Chabrier IMF).

panel is a smoothed version of the upper panel, produced via local-weighted regression smoothing (LOESS; Cleveland & Devlin 1988) as implemented in IDL.[4] We find $12 + \log(\mathrm{O/H})_\mathrm{e}$ and $\log(\mathrm{N/O})_\mathrm{e}$ to themselves correlate tightly ($\rho = 0.97$). Thus, we quantify the variation of Φ_e across chemical space using partial correlation coefficients $\rho_{ij,k}$, which have been applied in multiple recent galaxy studies (e.g, Bait, Barway & Wadadekar 2017; Bluck et al. 2020; Baker et al. 2022); in this notation, the correlation is calculated between parameters i and j with a third parameter k controlled for.

We employ partial correlation coefficients to determine the direction of maximum increase for Φ_e, which we present as an arrow in Figure 3. We detect a significant correlation between $\log(\mathrm{N/O})_\mathrm{e}$ and Φ_e with $\log(\mathrm{O/H})_\mathrm{e}$ accounted for, but we detect very little residual trend between $\log(\mathrm{O/H})_\mathrm{e}$ and Φ_e when $\log(\mathrm{N/O})_\mathrm{e}$ is accounted for. Such a result is also apparent visually from the smoothed Φ_e values: Φ_e varies very little with $\log(\mathrm{O/H})_\mathrm{e}$ at a given $\log(\mathrm{N/O})_\mathrm{e}$, in spite of the strong metallicity correlations shown in Figure 2.

3.1 Comparison with fibre-based abundances

Our use of 1 R_e annulus abundances is a crucial aspect of this work. Our sample possesses a median $\log(R_\mathrm{e}/\mathrm{kpc})$ of 0.61 and hence extends to sizes far above the region of sufficient fibre coverage in D'Eugenio et al. (2018) [$\log(R_\mathrm{e}/\mathrm{kpc}) \lesssim 0.5$ at $\log(M_*/\mathrm{M}_\odot) > 10$; their fig. 5]. To further quantify this point, we obtained r-band Petrosian half-light radii (R_{50}) from the NSA catalogue. We found 889 galaxies (43 per cent of our sample) to possess $R_\mathrm{fib}/R_{50} < 0.5$, where R_fib indicates the 3″ SDSS fibre radius, which in D'Eugenio et al. (2018) signifies insufficient coverage. Consequently, it can immediately be expected that our results for these galaxies would *not* hold were SDSS fibre-based measurements to be used for this sample.

We investigated fibre measurements by cross-matching our sample with MPA-JHU fibre emission line fluxes, processed in the same manner described for MaNGA spaxel measurements in Section 2. We restricted the test to galaxies satisfying BPT requirements along with satisfying $EW_{\mathrm{H}\alpha} > 14$ Å and S/N requirements, which reduces the sample to 754 objects. We found O/H and N/O to correlate more strongly with M_* ($\rho = 0.72, 0.77$ for O/H, N/O) than with Φ_e ($\rho = 0.66, 0.74$ for O/H, N/O) or Σ_e ($\rho = 0.41, 0.47$ for O/H, N/O), which disagrees with our MaNGA analysis. Restricting to the 567 galaxies for which $R_\mathrm{fib}/R_{50} \geq 0.5$, we found O/H and N/O to correlate more similarly with M_* ($\rho = 0.71, 0.75$ for O/H, N/O) than with Φ_e ($\rho = 0.68, 0.75$ for O/H, N/O), though we still do not reproduce the findings of D'Eugenio et al. (2018) or of our main analysis. Sample selection differences are a possible reason for the discrepancy with D'Eugenio et al. (2018) in this case. Nonetheless, it is clear that our use of 1 R_e abundances is an important aspect of our analysis.

4 DISCUSSION & CONCLUSIONS

We have demonstrated a tight correlation between the N/O chemical abundance in galaxies and the Φ_e parameter (M_*/R_e). We have further demonstrated that this trend is tighter than previously reported correlations between Φ_e and gas metallicity, for which we in fact detect very little connection once N/O is accounted for via partial correlation coefficients.

Our results, we note, hold over a range of calibrators. In particular, we obtain very similar results if we instead use the Curti et al. (2020) O3N2 or R23 calibrators to obtain gaseous metallicities.[5] Our results are also very similar if we instead use the N2S2 calibrator of Pérez-Montero & Contini (2009) (their equation 22) to obtain N/O abundances. We obtained different results when using metallicities derived from the Curti et al. (2020) N2 calibrator or the Dopita et al. (2016) N2S2Hα calibrator: in both cases, we find potential to trend primarily with O/H with little residual N/O dependence when the N2O2 indicator is used. Such a difference is not surprising: the N2 and N2S2Hα calibrators rely heavily on nitrogen emission features and will be insensitive to O/H variations at fixed N/O, making them less appropriate for our analysis than nitrogen-independent indicators such as RS32 or R23 (see also Schaefer et al. 2020).[6]

The Φ_e–metallicity relation has previously been interpreted as reflecting the importance of escape velocity (D'Eugenio et al. 2018; Sánchez-Menguiano et al. 2024), with Φ_e understood as a proxy for a galaxy's gravitational potential. Higher values of Φ_e would be expected to correspond to higher escape velocities, with higher escape velocities conferring greater resistance to metal-loss via outflows; this in turn is expected to lead to higher measured metallicities (e.g. Tremonti et al. 2004).

Baker & Maiolino (2023) however argue for an alternative scenario. They report gas metallicities to correlate more tightly with M_* than with dynamical mass M_dyn or with $M_\mathrm{dyn}/R_\mathrm{e}$, where M_dyn is derived from the Jeans Anisotropic Mass modelling (Cappellari 2008) analysis of Li et al. (2018). Baker & Maiolino (2023) therefore argue for a scenario in which metallicity is driven primarily by the integral of metal production within a galaxy, with the mass–metallicity relation emerging as a direct consequence.

The Baker & Maiolino (2023) scenario effectively treats both M_* and metallicity as time indicators: galaxies grow in mass over time while also enriching over time, thus resulting in more massive

[4] Available from http://www-astro.physics.ox.ac.uk/~mxc/software/. We compute smoothed values using the closest 10 per cent of data points with the *rescale* keyword applied, and errors using the scatter in neighbouring points.

[5] These both overlap with N2O2 in terms of employed emission lines, leading us to prefer RS32 for our main analysis.

[6] We note that the form of the N2S2Hα index (N2S2 − 0.264N2) produces an especially tight correlation with the N2S2 index, making N2S2Hα metallicities particularly ill-suited for considering N/O and O/H together.

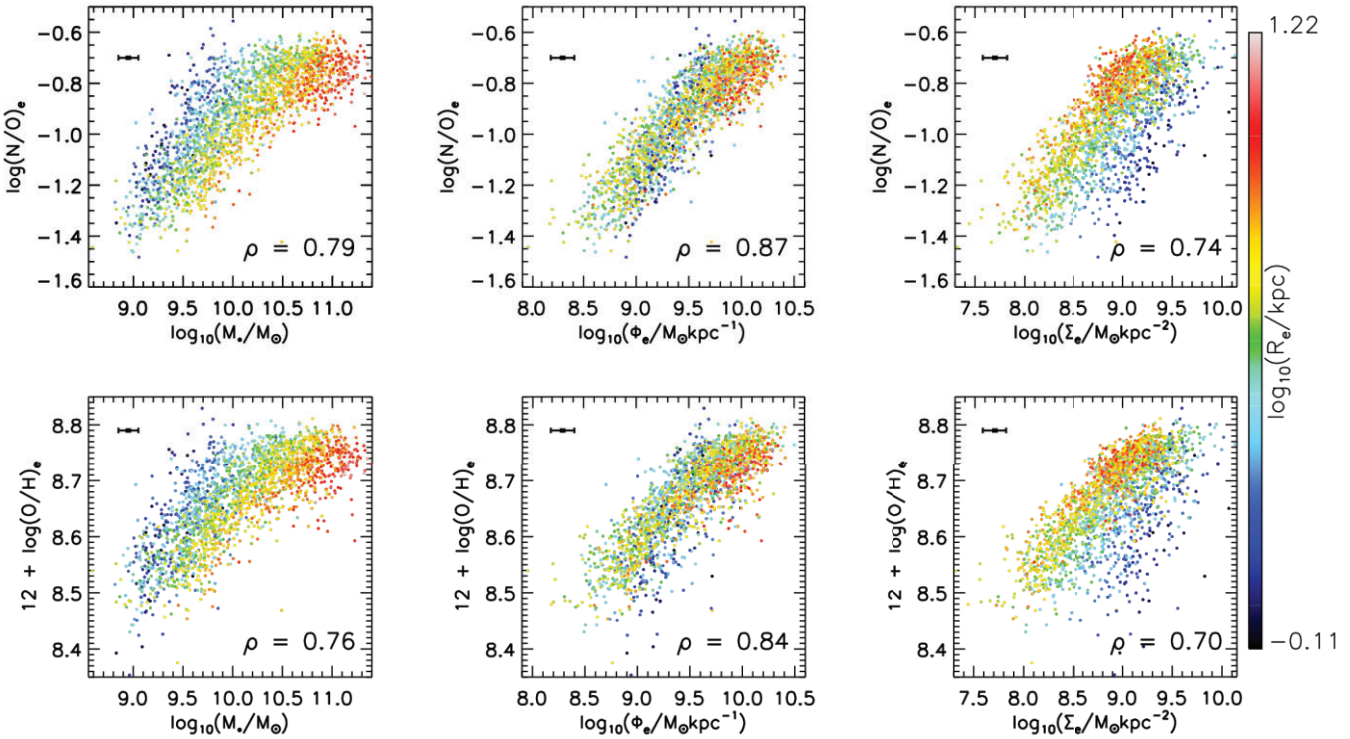

Figure 2. N/O abundances (top) and gas metallicities (bottom), at 1 R_e, as functions of M_* (left panels), Φ_e (middle panels), and Σ_e (right panels). Each panel displays the corresponding Spearman correlation coefficient ρ, all with $P \ll 0.01$. We colour data points by galaxies' R_e, with error bars showing the median uncertainties.

galaxies being more metal-rich. It should be noted however that the Baker & Maiolino (2023) scenario cannot *in itself* explain the observed inverse trend between metallicity and size *at a given stellar mass* (e.g. Ellison et al. 2008; D'Eugenio et al. 2018; Sánchez-Menguiano et al. 2024), with the Φ_e parameter having not been considered in their analysis. Furthermore, this scenario does not directly consider the roles of gaseous inflows and outflows (e.g. Schmidt 1963; Lilly et al. 2013; Barrera-Ballesteros et al. 2018; Yang, Scholte & Saintonge 2024), both of which can be expected to lead to scatter in the mass–metallicity relation. These sources of scatter can be understood as follows:

(i) Variations in gaseous inflow rates at a given stellar mass, producing short-term changes in galaxies' gas metallcities.
(ii) Variations in gaseous outflow rates at a given stellar mass, driven by variations in escape velocity; this would lead to longer term differences in galaxies' gas metallicities.

Both sources of scatter, we argue, are significantly reduced if one instead considers the Φ_e–N/O relation:

(i) Gaseous inflows can typically be expected to be metal-poor, and so they primarily affect the hydrogen content. Thus, by considering N/O instead of O/H, the scatter in measured relations is reduced.
(ii) Escape velocity variations will correspond to variations in gravitational potential, with gravitational potential encoded within the Φ_e parameter. Thus, by considering Φ_e instead of M_*, the scatter in measured relations is further reduced.

Given the time delay between oxygen and nitrogen enrichment, star-formation histories (SFHs) are another important consideration (e.g. Edmunds & Pagel 1978; Mollá et al. 2006; Vincenzo et al. 2016; Matthee & Schaye 2018). Φ_e can be expected to encode SFH information more effectively than M_*, with more compact star-forming galaxies found to be older at a given stellar mass (e.g. Li et al. 2018; Barone et al. 2020). Φ_e is in fact found to correlate more closely than Σ_e or M_* to MaNGA pipe3d (Sánchez et al. 2022) light-weighted stellar ages at 1 R_e (Boardman et al. in preparation). If higher-Φ_e galaxies are typically older, with a greater proportion of stars formed at earlier times, then this would confer greater nitrogen production (at fixed metallicity) from previous generations of stars. An N/O–SFH connection could also explain trends between N/O and SFR at fixed M_* (Hayden-Pawson et al. 2022), as well as explaining radial abundance profiles of individual galaxies along the N/O–O/H plane (Pilyugin & Tautvaišienė 2024).

Given the above, we argue the extremely tight Φ_e–N/O relation to be due to several factors. Firstly, Φ_e indeed encodes information about galaxy mass and hence about the integral of metal production, producing a positive Φ_e–N/O correlation. Secondly, Φ_e encodes information about escape velocities and thus accounts for some of the scatter in the mass–metallicity relation. Thirdly, variations in Φ_e *at a given metallicity* will correspond in part to age variations, with older galaxies expected to experience greater nitrogen enrichment at a given metallicity. Finally, variations in metal-poor inflow rates can be expected to significantly impact O/H abundances on short time-scales, with N/O abundances comparatively unaffected (see Section 1); this is because metal-poor inflows mostly increase the abundance of hydrogen while having far less impact on heavier elements' relative abundances. Thus, while O/H and N/O both serve as indicators of chemical evolution, N/O is less impacted by short time-scale events such as recent inflow, leading to a more robust connection to overall galactic chemical enrichment.

To summarize, we report in this letter a notably tight Φ_e–N/O relation detected in MaNGA galaxies. This relation is tighter than

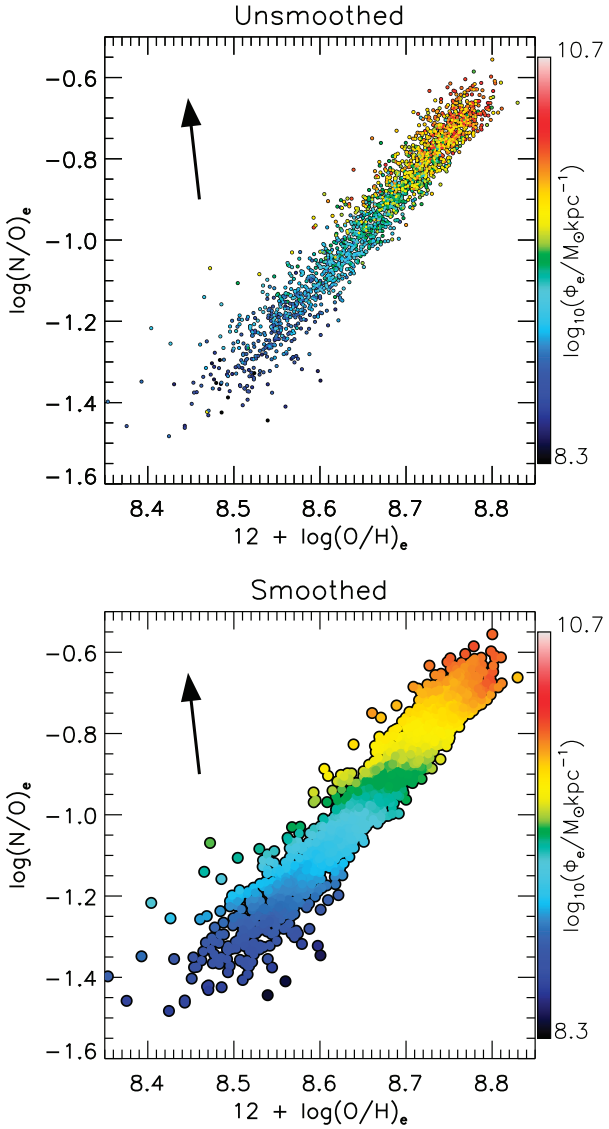

Figure 3. Potential Φ_e as a combined function of $\log(N/O)_e$ and $12 + \log(O/H)_e$, before (top) and after (bottom) applying LOESS smoothing. The black arrow represents the direction of increasing Φ_e in N/O–O/H space and is computed via partial correlation coefficients.

both the mass–metallicity relation and the Φ_e–metallicity relation. The Φ_e–N/O relation also appears more fundamental, in the sense that only a mild Φ_e–metallicity correlation is found once the N/O abundance is accounted for. We argue these results are due to Φ_e encoding information about both SFHs and escape velocities in addition to M_*, with N/O being relatively insensitive to metal-poor inflows.

ACKNOWLEDGEMENTS

NFB and VW acknowledge Science and Technologies Facilities Council (STFC) grant ST/V000861/1. NVA and VW acknowledge the Royal Society and the Newton Fund via the award of a Royal Society – Newton Advanced Fellowship (grant NAF\R1\180403). NVA acknowledges support from Conselho Nacional de Desenvolvimento Científico e Tecnológico (CNPq). Funding for the Sloan Digital Sky Survey IV has been provided by the Alfred P. Sloan Foundation, the U.S. Department of Energy Office of Science, and the Participating Institutions. SDSS-IV acknowledges support and resources from the Center for High-Performance Computing at the University of Utah. The SDSS web site is www.sdss.org.

SDSS-IV is managed by the Astrophysical Research Consortium for the Participating Institutions of the SDSS Collaboration including the Brazilian Participation Group, the Carnegie Institution for Science, Carnegie Mellon University, the Chilean Participation Group, the French Participation Group, Harvard-Smithsonian Center for Astrophysics, Instituto de Astrofísica de Canarias, The Johns Hopkins University, Kavli Institute for the Physics and Mathematics of the Universe (IPMU) / University of Tokyo, Lawrence Berkeley National Laboratory, Leibniz Institut für Astrophysik Potsdam (AIP), Max-Planck-Institut für Astronomie (MPIA Heidelberg), Max-Planck-Institut für Astrophysik (MPA Garching), Max-Planck-Institut für Extraterrestrische Physik (MPE), National Astronomical Observatories of China, New Mexico State University, New York University, University of Notre Dame, Observatário Nacional / MCTI, The Ohio State University, Pennsylvania State University, Shanghai Astronomical Observatory, United Kingdom Participation Group, Universidad Nacional Autónoma de México, University of Arizona, University of Colorado Boulder, University of Oxford, University of Portsmouth, University of Utah, University of Virginia, University of Washington, University of Wisconsin, Vanderbilt University, and Yale University.

DATA AVAILABILITY

All data used here are publicly available.

REFERENCES

Abdurro'uf et al., 2022, ApJS, 259, 35
Andrews B. H., Martini P., 2013, ApJ, 765, 140
Bait O., Barway S., Wadadekar Y., 2017, MNRAS, 471, 2687
Baker W. M., Maiolino R., 2023, MNRAS, 521, 4173
Baker W. M., Maiolino R., Bluck A. F. L., Lin L., Ellison S. L., Belfiore F., Pan H.-A., Thorp M., 2022, MNRAS, 510, 3622
Baldwin J. A., Phillips M. M., Terlevich R., 1981, PASP, 93, 5
Barone T. M. et al., 2018, ApJ, 856, 64
Barone T. M., D'Eugenio F., Colless M., Scott N., 2020, ApJ, 898, 62
Barone T. M. et al., 2022, MNRAS, 512, 3828
Barrera-Ballesteros J. K. et al., 2018, ApJ, 852, 74
Belfiore F. et al., 2019a, AJ, 158, 160
Belfiore F., Vincenzo F., Maiolino R., Matteucci F., 2019b, MNRAS, 487, 456
Blanton M. R., Kazin E., Muna D., Weaver B. A., Price-Whelan A., 2011, AJ, 142, 31
Bluck A. F. L. et al., 2020, MNRAS, 499, 230
Boardman N. F., Zasowski G., Newman J. A., Sanchez S. F., Schaefer A., Lian J., Bizyaev D., Drory N., 2021, MNRAS, 501, 948
Boardman N. et al., 2022, MNRAS, 514, 2298
Bundy K. et al., 2015, ApJ, 798, 7
Cappellari M., 2008, MNRAS, 390, 71
Chabrier G., 2003, PASP, 115, 763
Cherinka B. et al., 2019, AJ, 158, 74
Cleveland W. S., Devlin S. J., 1988, J. Am. Stat. Assoc., 83, 596
Curti M., Mannucci F., Cresci G., Maiolino R., 2020, MNRAS, 491, 944
D'Eugenio F., Colless M., Groves B., Bian F., Barone T. M., 2018, MNRAS, 479, 1807
Dopita M. A., Kewley L. J., Sutherland R. S., Nicholls D. C., 2016, Ap&SS, 361, 61
Drory N. et al., 2015, AJ, 149, 77
Edmunds M. G., Pagel B. E. J., 1978, MNRAS, 185, 77P

Ellison S. L., Patton D. R., Simard L., McConnachie A. W., 2008, ApJ, 672, L107
Fitzpatrick E. L., Massa D., Gordon K. D., Bohlin R., Clayton G. C., 2019, ApJ, 886, 108
Florido E., Zurita A., Pérez-Montero E., 2022, MNRAS, 513, 2006
Gallazzi A., Charlot S., Brinchmann J., White S. D. M., Tremonti C. A., 2005, MNRAS, 362, 41
González Delgado R. M. et al., 2014, A&A, 562, A47
González Delgado R. M. et al., 2015, A&A, 581, A103
Gunn J. E. et al., 2006, AJ, 131, 2332
Hayden-Pawson C. et al., 2022, MNRAS, 512, 2867
Kauffmann G. et al., 2003, MNRAS, 346, 1055
Kewley L. J., Ellison S. L., 2008, ApJ, 681, 1183
Kewley L. J., Heisler C. A., Dopita M. A., Lumsden S., 2001, ApJS, 132, 37
Lacerda E. A. D. et al., 2018, MNRAS, 474, 3727
Law D. R. et al., 2015, AJ, 150, 19
Law D. R. et al., 2016, AJ, 152, 83
Law D. R. et al., 2021, AJ, 161, 52
Lequeux J., Peimbert M., Rayo J. F., Serrano A., Torres-Peimbert S., 1979, A&A, 500, 145
Li H. et al., 2018, MNRAS, 476, 1765
Lilly S. J., Carollo C. M., Pipino A., Renzini A., Peng Y., 2013, ApJ, 772, 119
Ma H.-C., Du M., Ho L. C., Sheng M.-j., Liao S., 2024, A&A, preprint (arXiv:2404.10432)
Maiolino R., Mannucci F., 2019, A&AR, 27, 3
Matthee J., Schaye J., 2018, MNRAS, 479, L34
McDermid R. M. et al., 2015, MNRAS, 448, 3484
Mollá M., Vílchez J. M., Gavilán M., Díaz A. I., 2006, MNRAS, 372, 1069
O'Donnell J. E., 1994, ApJ, 422, 158
Osterbrock D. E., Pogge R. W., 1985, ApJ, 297, 166
Pérez-Montero E., Contini T., 2009, MNRAS, 398, 949
Pérez-Montero E. et al., 2016, A&A, 595, A62
Pilyugin L. S., Tautvaišienė G., 2024, A&A, 682, A41
Pilyugin L. S., Vílchez J. M., Thuan T. X., 2010, ApJ, 720, 1738
Sánchez-Menguiano L., Sánchez Almeida J., Sánchez S. F., Muñoz-Tuñón C., 2024, A&A, 681, A121
Sánchez S. F. et al., 2016a, Rev. Mex. Astron. Astrofis., 52, 21
Sánchez S. F. et al., 2016b, Rev. Mex. Astron. Astrofis., 52, 171
Sánchez S. F. et al., 2018, Rev. Mex. Astron. Astrofis., 54, 217
Sánchez S. F. et al., 2022, ApJS, 262, 36
Schaefer A. L., Tremonti C., Belfiore F., Pace Z., Bershady M. A., Andrews B. H., Drory N., 2020, ApJ, 890, L3
Schlegel D. J., Finkbeiner D. P., Davis M., 1998, ApJ, 500, 525
Schmidt M., 1963, ApJ, 137, 758
Scudder J. M., Ellison S. L., El Meddah El Idrissi L., Poetrodjojo H., 2021, MNRAS, 507, 2468
Smee S. A. et al., 2013, AJ, 146, 32
Timmes F. X., Woosley S. E., Weaver T. A., 1995, ApJS, 98, 617
Tremonti C. A. et al., 2004, ApJ, 613, 898
Vale Asari N., Couto G. S., Cid Fernandes R., Stasińska G., de Amorim A. L., Ruschel-Dutra D., Werle A., Florido T. Z., 2019, MNRAS, 489, 4721
Vaughan S. P. et al., 2022, MNRAS, 516, 2971
Veilleux S., Osterbrock D. E., 1987, ApJS, 63, 295
Vincenzo F., Belfiore F., Maiolino R., Matteucci F., Ventura P., 2016, MNRAS, 458, 3466
Wake D. A. et al., 2017, AJ, 154, 86
Westfall K. B. et al., 2019, AJ, 158, 231
Yan R. et al., 2016a, AJ, 151, 8
Yan R. et al., 2016b, AJ, 152, 197
Yang N., Scholte D., Saintonge A., 2024, MNRAS, 527, 11043

This paper has been typeset from a TEX/LATEX file prepared by the author.